Maximum Carrying Capacity and Granular Temperature of A, B and C Particles

Dimitri Gidaspow and Reza Mostofi
Chemical and Environmental Engineering Dept., Illinois Institute of Technology, Chicago, IL 60616

The observed cyclic operation of a riser near choking was calculated using a computational fluid-dynamic model used previously to predict its flow regimes. An approximate analytical expression for the maximum carrying capacity of Geldart A, B and C particles was developed and compared to data in the literature. In the new theory, an unknown parameter is the pseudosonic velocity of the particles. To estimate this quantity, new granular temperatures were measured and compared to data from the literature for Geldart A, B and C particles. In the riser flow regime (2% to 20% solid volume fraction), the turbulent intensity of the particles is approximately 0.5, in agreement with the theory. The theoretical value involves the ratio of particle viscosity to the granular conductivity.

Introduction

The flow of particles in a vertical pipe is a common unit operation in the chemical and petroleum industries. For example, in fluid catalytic cracking (FCC), oil droplets and steam are introduced into the riser carrying the FCC catalyst, to produce low molecular-weight compounds, such as gasoline (Avidan, 1997, 2001; Squires et al., 1985). The theory of riser operation is not yet complete. In response to this challenge, a Multiphase Fluid Dynamics Research Consortium (MFDRC) was formed (Thompson, 2000). It consists of six national laboratories, six universities, and American chemical companies, led by Dow Chemical.

The maximum carrying capacity of a riser is the maximum steady-state flux of a solid for a given gas velocity. In the transport of solids in a vertical pipe, the pressure drop as a function of inlet superficial gas velocity has the shape shown in Figure 1a. This figure is similar to Figure 10.4 of Zenz and Othmer (1960). The choking velocity is the asymptote of the pressure-drop curve. As the gas velocity approaches this choking velocity, the pressure drop undergoes wild oscillations. Figure 1b shows the behavior of the pressure-drop oscillations as choking is approached by decreasing the gas velocity. Figure 1c shows the solid mass flux at choking vs. superficial gas velocity.

In the absence of a reliable theory, such fluxes are determined experimentally using costly experimental setups. For example, recently such saturated carrying capacities were determined at NETL in Morgantown for the transport of cork that simulates the transport of coal particles (Shadle et al., 2002).

The most thorough review of the theory of choking and empirical choking correlations can be found in Leung (1980). More recently, Bi et al. (1993) recognized three types of choking mechanisms. In this article, we limit ourselves to their type C only. Yousfi and Gau (1974) obtained a choking correlation partially based on a hydrodynamic instability analysis of a wave equation for the voidage. Yousfi and Gau's correlation involves the diameter of particles. Yang (1975, 1983) introduced the diameter of the pipe into his semiempirical correlations through the use of the slugging velocity in a pipe. Takeuchi et al. (1986) obtained a quantitative flux regime map for FCC particles. Satija et al. (1985) emphasized the increase in pressure-drop amplitude as choking is approached. Knowlton and Bachovchin (1976) included the effect of gas density into their empirical correlation.

In this article we present a computational fluid dynamics (CFD) computation of riser behavior near choking. We also present approximate analytical expressions for choking velocity and flux based on the concept of resonance. It is well known in vibration analysis that resonance occurs when the imposed frequency is set to the natural frequency of the object. At resonance the amplitude of the vibration becomes unbounded. This corresponds to the pressure drop increase as shown in Figure 1a.

Correspondence concerning this article should be addressed to D. Gidaspow.

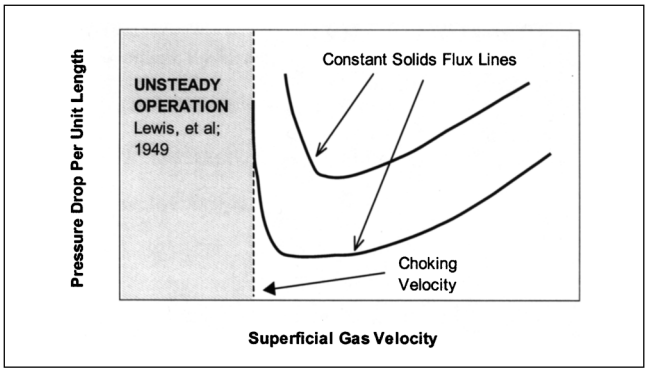

(a)

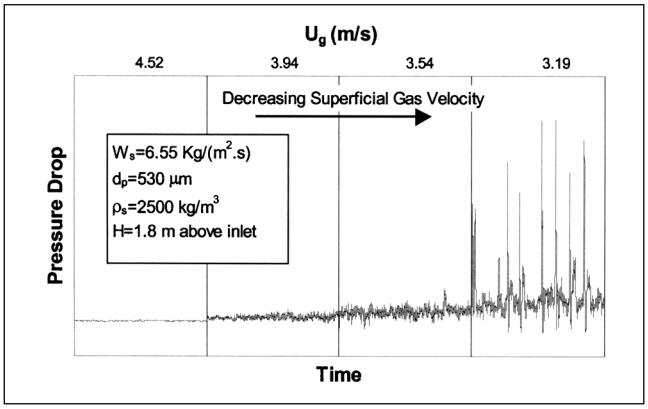

(b)

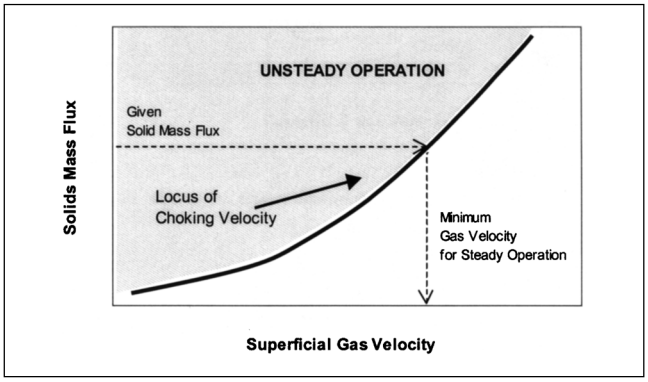

(c)

Figure 1. (a) Determination of choking velocity; (b) pressure drop oscillations as choking is approached at a constant solids flux in the IIT riser (Tartan and Gidaspow, 2002); (c) maximum carrying capacity of particles.

CFD Simulation for the Unsteady Regime

A numerical model shown previously (Sun and Gidaspow, 1999) to correctly describe flow regimes in a riser in the CFB regime is used here to model the riser unsteady behavior near choking. Hence here we demonstrate the capability of the computer model to predict the behavior of the two flow regimes, as qualitatively depicted in Figure 1. The locus of the choking velocity lies between the unsteady operation described here and the previous modeling of CFB (Sun and Gidaspow, 1999). Table 1 summarizes the mass and momentum balances and the constitutive equations used in this simulation. This set of equations corresponds to model B in Gidaspow's (1994) book. Figure 2 shows the diagram of the riser, and Table 2 summarizes the simulation conditions. The dimensions of the riser used are those of the PSRI riser given for the Challenge II problem for Fluidization X. The riser was simulated in two dimensions.

Figures 3 and 4 show the average outlet flux and the average bed density as a function of time, respectively. Figure 5 shows the bed density and the volume fractions as a function of time. The particles gradually fill the pipe and then are blown out quickly. The process repeats itself. Lewis et al. experimentally observed such behavior as early as 1949. They stated: "Instead of obtaining a steady-state condition, the solid concentration in the fluidizing unit continually increased until the bed was of very high density. There would be a sudden surge which would blow most of this solid out of the unit and the cycle would be repeated." The volume fraction distribution shows that there is a sluglike behavior, as earlier postulated by Yang (1975, 1983). At the maximum bed density the pressure drop is also a maximum, so at this point the pressure at the bottom is the highest. Therefore, this high-pressure buildup causes the sudden emptying of the pipe. A video of the simulation is available on the Web site, www.chee.iit.edu/faculty/gidaspow.htm.

At higher gas velocities as shown for the Challenge II problem, submitted for Fluidization X (Gidaspow and Mostofi, 2001), the behavior of the system is in the usual circulating fluidized-bed regime. The amplitudes of oscillations are relatively small compared to the time-average values. Similar simulations were performed by Benyahia et al. (1998), Benyahia and Arastoopour (2001), Guenther et al. (2001), Mathiesen et al. (1999), and Kuippers et al. (1998).

Analytical Expression for Frequencies

In this section we derive an equation for the forced and natural frequencies oscillations in the vertical pipe. We begin with the momentum balance for the solids equation (fourth equation) in Table 1. To obtain an analytical solution for the frequency, a number of approximations are necessary. First, we neglect the velocity square terms. This simplification will immediately lead to the neglect of v_s compared to C_s in the wave-propagation analysis. We further restrict the analysis to flow of particles above minimum fluidization. This leads to the neglect of solids stress caused by particle contact, except those caused by collisions. With these simplifications the solids momentum balance for phase s becomes as follows. Symbols are those in Gidaspow (1994)

$$\frac{\partial(\epsilon_s \rho_s v_s)}{\partial t} = -\frac{\partial P_s}{\partial x} - \epsilon_s g(\rho_s - \rho_g) - \beta(v_s - v_g). \quad (1)$$

Acceleration of Momentum of Phase s | Solids Pressure due to Collisions | Buoyancy | Drag

Note that for a steady state with a negligible solids pressure, Eq. 1 is the conventional balance of buoyancy and drag. Here,

Table 1. Hydrodynamic Model

Gas-phase continuity	$\frac{\partial}{\partial t}(\epsilon_g \rho_g)+\nabla\cdot(\epsilon_g \rho_g \boldsymbol{v}_g)=0$
Solid-phase continuity	$\frac{\partial}{\partial t}(\epsilon_s \rho_s)+\nabla\cdot(\epsilon_s \rho_s \boldsymbol{v}_s)=0$
Gas-phase momentum	$\frac{\partial}{\partial t}(\epsilon_g \rho_g \boldsymbol{v}_g)+\nabla\cdot(\epsilon_g \rho_g \boldsymbol{v}_g \boldsymbol{v}_g)=-\nabla P_g+\nabla \boldsymbol{T}_g+\rho_g \boldsymbol{g}+\beta(\boldsymbol{v}_s-\boldsymbol{v}_g)$
Solid-phase momentum	$\frac{\partial}{\partial t}(\epsilon_s \rho_s \boldsymbol{v}_s)+\nabla\cdot(\epsilon_s \rho_s \boldsymbol{v}_s \boldsymbol{v}_s)=\nabla \boldsymbol{T}_s+\epsilon_s(\rho_s-\rho_g)\boldsymbol{g}-\beta(\boldsymbol{v}_s-\boldsymbol{v}_g)$
Ideal gas law	$P_g=\rho_g \tilde{R} T_g$
Gas-phase stress tensor	$\boldsymbol{T}_g=2\epsilon_g \mu_g\left\{\frac{1}{2}\left[\nabla \boldsymbol{v}_g+(\nabla \boldsymbol{v}_g)^T\right]-\frac{1}{3}(\nabla\cdot \boldsymbol{v}_g)\boldsymbol{I}\right\}$
Solid-phase stress tensor	$\boldsymbol{T}_s=(-P_s+\xi_s\nabla\cdot \boldsymbol{v}_s)\boldsymbol{I}+2\mu_s\left\{\frac{1}{2}[\nabla \boldsymbol{v}_s+(\nabla \boldsymbol{v}_s)^T]-\frac{1}{3}(\nabla\cdot \boldsymbol{v}_s)\boldsymbol{I}\right\}$
Solids pressure	$\nabla P_s=G(\epsilon_g)\nabla\epsilon_g \quad$ where $\quad G(\epsilon_g)=10^{-8.686\epsilon_g+8.577}$
Solids viscosity	$\xi_k=0 \qquad \mu_s=5.0\times\epsilon_s$
Drag coefficient $\epsilon_g \geq 0.8$	$\beta=\frac{3}{4}C_d\frac{\epsilon_s \rho_g \lvert\boldsymbol{v}_g-\boldsymbol{v}_s\rvert}{d_s}\epsilon_g^{-2.65}$
	$C_d=\frac{24}{Re_s}(1+0.15Re_s^{0.687}) \qquad Re_s<1{,}000$
	$C_d=0.44 \qquad Re_s\geq 1{,}000$
	$Re_s=\frac{\epsilon_g \rho_g d_s \lvert\boldsymbol{v}_g-\boldsymbol{v}_s\rvert}{\mu_g}$
Drag coefficient $\epsilon_g < 0.8$	$\beta=150\frac{\epsilon_s^2\mu_g}{\epsilon_g^2 d_p^2}+1.75\frac{\rho_g \epsilon_s \lvert\boldsymbol{v}_g-\boldsymbol{v}_s\rvert}{d_s \epsilon_g}$

however, we emphasize the time variation. Hence, we need the transient conservation of the particles equation, which is as follows in one dimension:

$$\frac{\partial(\epsilon_s \rho_s)}{\partial t}+\frac{\partial(\epsilon_s \rho_s v_s)}{\partial x}=0. \tag{2}$$

A wave equation for the bulk density $\rho_B=\rho_s\epsilon_s$ or for the flux, $F=\rho_s\epsilon_s v_s$ can be obtained by following the procedure in chapter 7 in Gidaspow's book

$$\frac{\partial^2\rho_B}{\partial t^2}=C_s^2\frac{\partial^2\rho_B}{\partial x^2}+g\frac{\partial\rho_B}{\partial x}-\beta\left(\frac{\partial v_g}{\partial x}-\frac{\partial v_s}{\partial x}\right). \tag{3}$$

Wave Propagation — Source — Drag (Zero for Developed Flow)

Equation 3 shows that the density wave propagates with the pseudosonic velocity C_s (Savage, 1988), that gravity acts as a source for wave formation, and that drag dampens the waves, when the relative velocity is positive. Generalization of Eq. 3 to two and three dimensions shows that there will be additional source terms due to gradients of (v_g-v_s) in the multiple dimensions. These terms may give additional peaks in the spectral analysis of bulk density. For developed flow the axial variation of the relative velocity becomes zero in Eq. 3. Further, if we neglect the solids pressure effect, the sonic velocity, Eq. 3 simplifies to a diffusion equation

$$\frac{\partial^2\rho_B}{\partial t^2}=g\frac{\partial\rho_B}{\partial x}. \tag{4}$$

The variation of bulk density with height, x, is obtained from an additional momentum balance. For developed one-dimensional (1-D) flow the pressure drop is balanced approximately by the weight of the bed, which is expressed by

$$\frac{\partial P}{\partial x}=g\rho_B. \tag{5}$$

The pressure drop itself is given by the Ergun equation, which for small relative velocities is as follows

$$-\frac{dP}{dx}=\frac{150\mu_g}{(\phi d_p)^2}\frac{\epsilon_s^2}{\epsilon^3}U_o. \tag{6}$$

We now relate the pressure drop to relative bed expansion using the method of Thompson (1978), who obtained a formula for frequency similar to that derived here. Thompson did not use conventional fluidization equations, but constructed a flow model of his own.

The 1-D conservation of particles balance moving with a constant mass is as follows

$$\frac{d}{dt}\int_o^{x(t)}\rho_s\epsilon_s\,dx=0. \tag{7a}$$

Differentiation of Eq. 7a using the Leibniz rule (Gidaspow, 1994, appendix C) gives Eq. 2. Integration of Eq. 7a moving with a constant mass for constant particle density produces the integral shown in Eq. 7b below

$$\int_0^{x(t)}\epsilon_s dx=\epsilon_{so}x_o. \tag{7b}$$

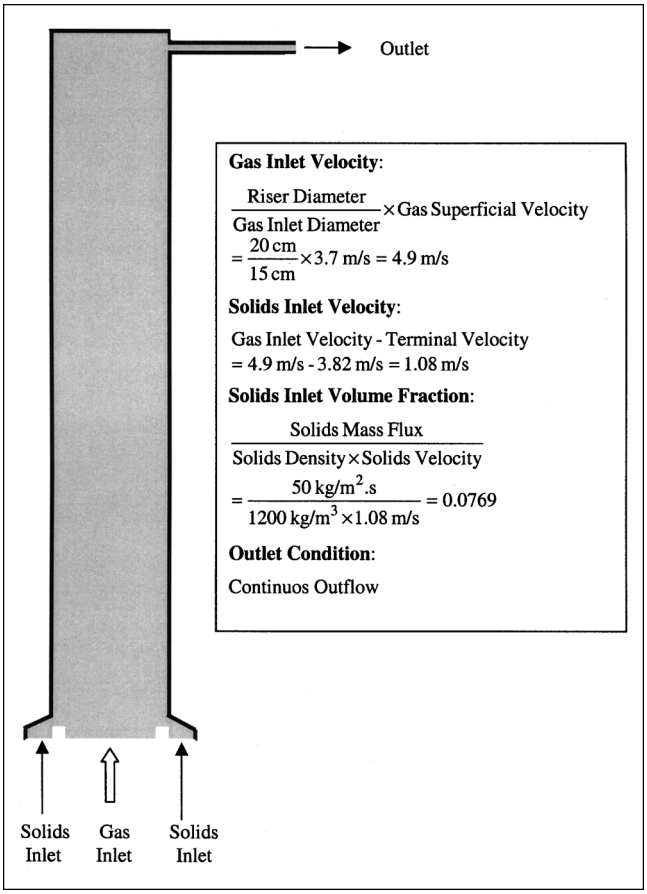

Figure 2. Riser and boundary conditions.

An application of the mean-value theorem to Eq. 7b shows that

$$\epsilon_{s,\text{mean}} x(t) = \epsilon_{so} x_o, \tag{7c}$$

where $\epsilon_{s,\text{ mean}}$ is the average volume fraction of particles in the bed, and ϵ_{so} and x_o are some initial bed volume fraction and height of bed filled with particles. For simplicity of writing, we call $\epsilon_{s,\text{ mean}}$ simply ϵ_s and $x(t)$, x. Using calculus, Eq. 7c gives the differential expression as

$$\frac{dx}{x} = -\frac{d\epsilon_s}{\epsilon_s}. \tag{8}$$

We now estimate the relative differential change of pressure using Eq. 6, as the volume fraction, ϵ_s, changes during the passage of a wave for a constant superficial velocity, U_o. By calculus only

$$\frac{d\left(\frac{dP}{dx}\right)}{\frac{dP}{dx}} = [3\epsilon_s/\epsilon + 2]\frac{d\epsilon_s}{\epsilon_s}. \tag{9}$$

Table 2. Simulation Conditions

Riser diameter	20 cm
Riser height	14.2 m
Particle size	67 μm
Particle density	1,200 kg/m^3
Solids mass flux	50 kg/m$^2\cdot$s
Gas superficial velocity	3.7 m/s
Grid no.	37 (radial) $\times$ 162 (axial)
Time step	$5.0e-06$

Using the differential particle balance, Eq. 8, the differential change of pressure drop can then be expressed as follows

$$\frac{d\left(\frac{dP}{dx}\right)}{dx} = -[3\epsilon_s/\epsilon + 2]\frac{\epsilon_s\left(\frac{dP}{dx}\right)}{\epsilon_{so} x_o}. \tag{10}$$

The preceding expression allows an estimate of the density gradient to be made.

Differentiation of Eq. 5 and substitution into Eq. 4 gives

$$\frac{\partial^2 \rho_B}{\partial t^2} = \frac{\partial^2 P}{\partial x^2}, \tag{11}$$

but

$$\frac{\partial^2 P}{\partial x^2} \approx \frac{\Delta\left(\frac{dP}{dx}\right)}{\Delta x}. \tag{12}$$

Using Eqs. 5 and 10, Eq. 11 becomes an ordinary differential equation

$$\frac{d^2\rho_B}{dt^2} + \left[\frac{(3\epsilon_s/\epsilon + 2)\epsilon_s g}{\epsilon_{so} x_o}\right]\rho_B = 0. \tag{13}$$

Equation 13 is the equation for the vibration of a spring of a unit mass, with the brackets representing a spring constant. Treating the bracket as a constant, the solution is

$$\rho_B = A\cos\omega t + B\sin\omega t, \tag{14}$$

where

$$\omega = \left(\frac{g}{x_o}\right)^{1/2}\left[\frac{(3\epsilon_s/\epsilon + 2)\epsilon_s}{\epsilon_{so}}\right]^{1/2}. \tag{15}$$

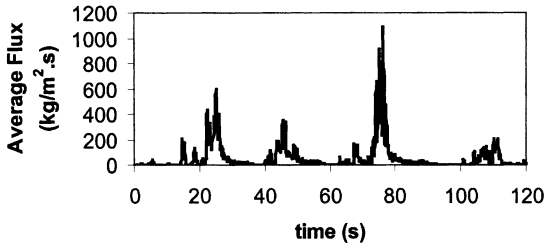

Figure 3. Output flux at different times.

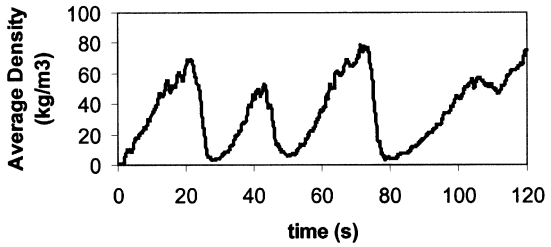

Figure 4. Large changes in instantaneous average bed density.

The forced frequency of oscillations, f, is

$$f = \frac{\omega}{2\pi}. \tag{16}$$

We see that the basic frequency is that caused by gravity, $(g/x_o)^{1/2}$, and that the frequency becomes very small as the volume fraction of particles becomes small. We showed (Gidaspow et al., 2001) that Eq. 15 compares very well with frequency data obtained by Baeyens and Geldart (1974) and others.

Verloop and Heertjes (1974) were the first to derive a frequency relation that has the basic term $(g/x_o)^{1/2}$ by treating a fluidized bed as a vibrating column. However, their relation does not have the correct compressibility term achieved by using some key steps contained in Thompson's (1978) analysis. In Eq. 13 the "elasticity" per unit mass is proportional to the volume fraction of the solid. A denser bed has a greater elasticity.

With the approximations made, Eq. 3 can be rewritten as

$$\frac{\partial^2 \rho_B}{\partial t^2} = C_s^2 \nabla^2 \rho_B + \underbrace{\left[\frac{(3\epsilon_s/\epsilon + 2)\,\epsilon_s g\,\rho_s}{\epsilon_{so} x_o}\right]}_{\text{Source}}. \tag{17}$$

The classic theory of wave propagation can be applied to this problem in the direction of flow. Equation 3 shows that at the boundaries, $x = 0$ and $x = x_o$, the gradient of bulk density is zero. Then separation of the variables of the homoge-

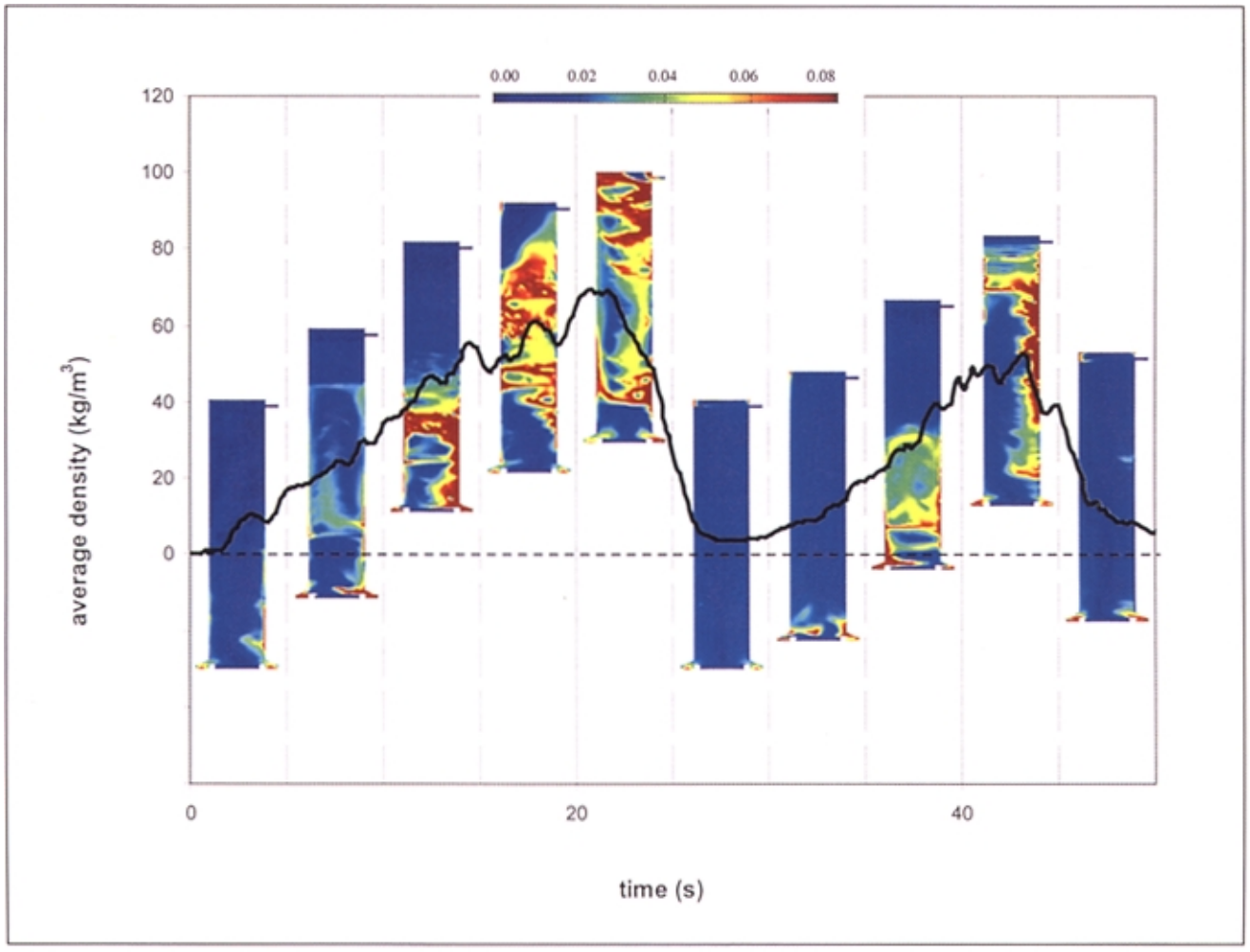

Figure 5. Riser behavior below choking velocity; solids volume fractions with the filling and emptying of the riser.

Table 3. Symbols in Figures 6 and 7

Symbol	Particle Size (mm)	Reference	Notes
A1	0.075	Miller and Gidaspow (1992)	From viscosity data
A2	0.075	Huilin and Gidaspow (1996)	From CCD camera
B1	0.283	Chen et al. (1994) Polashenski and Chen (1999)	Pressure transducer data and ideal equation of state
B2	0.500	Krishna, Jung and Gidaspow Jung (2002)	From CCD camera
B3	0.450	Gidaspow et al. (1999)	From CCD camera
B4	0.500	Campbell and Wang (1991)	Pressure transducer data and ideal equation of state
B5	2.800	Campbell and Wang (1991)	
B6	0.750	Campbell and Wang (1991)	
C1	0.040	Cody (1996)	Extrapolation data
C2	0.040	Krishna, MS Project Sharma (2002)	From CCD camera
C3	0.045	Jung and Gidaspow Jung (2002)	From CCD camera
C4	0.110; 0.500	Cody (1996)	
G1	—	Gidaspow (1994)	

neous portion of the wave equation is as follows. Let

$$\rho_B = T(t)X(x). \tag{18}$$

The ordinary differential equations become as follows, where prime denotes the derivative

$$\frac{T''}{T} = C_s^2\frac{X''}{X} = -\omega^2 \qquad T'' + \omega^2 T = 0 \qquad \text{and}$$

$$X'' + \frac{\omega^2}{C_s^2}X = 0, \tag{19}$$

with the boundary conditions

$$X'(0) = X'(x_o) = 0, \tag{20}$$

which give

$$X = A\cos\left(\frac{\omega_n}{C_s}\right)x \tag{21}$$

and the eigenvalues

$$\frac{\omega_n x_o}{C_s} = \pi n, \qquad n = 1,2,3,\ldots. \tag{22}$$

Hence, with the zero gradient boundary conditions, the fundamental frequency is

$$\omega_1 = \frac{\pi C_s}{x_o.} \tag{23}$$

In Eq. 23 C_s was relative to the velocity, v_s. Hence the natural frequency for the case when v_s is large compared with C_s can be expressed as

$$\omega_1 = \frac{\pi(v_s \pm C_s)}{x_o}. \tag{24}$$

A rigorous analysis of the 1-D equations for two-phase flow using the theory of characteristics shows that the characteristic directions are

$$v_s \pm C_s, \tag{25}$$

where the pseudosonic velocity (Savage, 1988) is

$$C_s = \sqrt{\frac{1}{\rho_s}}\left(\frac{\partial p_s}{\partial \epsilon_s}\right)^{1/2}. \tag{26}$$

Approximate Choking Formulas

The Navier–Stokes equations for compressible fluids (Table 1) can be decomposed into a wave equation for a potential with damping due to the fluid viscosity and into a stream function equation (Tolstoy, 1973; Morse and Feshbach, 1953). For zero viscosity that is for a high Reynolds number, the result is an undamped wave equation for a potential, which by substitution

$$\Phi(x,y,z)e^{-i\omega t} \tag{27}$$

can be transformed into the classic Helmholtz equation for the eigenfunction Φ_n

$$\nabla^2\Phi_n + k_n^2\Phi_n = 0, \tag{28}$$

where

$$k_n = \omega_n/C_s. \tag{29}$$

The corresponding equation for a unit-source solution, the Green's function, G_k, is

$$\nabla^2 G_k + k_{\text{source}}^2 = -4\pi\delta(\boldsymbol{r} - \boldsymbol{r}_{\text{source}}). \tag{30}$$

A standard Green's function construction (Morse and Feshbach, 1953) gives

$$G_k(\boldsymbol{r};\boldsymbol{r}_{\text{source}}) = 4\pi\sum_{n=1}^{\infty}\frac{\Phi_n(\boldsymbol{r})\Phi_n(\boldsymbol{r}_{\text{source}})}{k_n^2 - k_{\text{source}}^2}. \tag{31}$$

In Eq. 31 when

$$k_n = k_{\text{source}}, \tag{32}$$

we have a singularity. These are the infinities when a nondissipative vibrating system is driven at one of its resonant frequencies. For fluidization, the pressure drop goes to infinity.

Thus, resonance is obtained when a vibrating system is driven at one of its natural frequencies (Morse and Feshbach, 1953). Hence, we equate Eq. 15 to Eq. 24 to obtain the resonant condition (using L instead of x_o for simplicity)

$$\frac{(v_s \pm C_s)\pi}{L} = \left(\frac{g}{L}\right)^{1/2}\left[\frac{(3\epsilon_s/\epsilon + 2)\epsilon_s}{\epsilon_{so}}\right]^{1/2}. \tag{33}$$

Equation 33 relates the solids velocity at choking to the volume fraction at choking. These quantities are normally not measured, although it is possible to measure v_s using laser Doppler or CCD camera techniques. The volume fraction can be measured using gamma-ray or capacitance methods. To obtain the choking conditions we need to relate v_s to the superficial gas velocity. We used the concept of slip as done earlier by Yang (1975, 1983) and others (Leung, 1980).

We let

$$v_s = v_g - v_t, \tag{34}$$

where v_t is the terminal velocity. This relation is valid in dilute flow and is known to be inaccurate in the CFB regime, because of the core-annular structure of flow. We use it to obtain a simplified expression for choking, keeping its potential inaccuracy in mind. Then the choking velocity becomes

$$v_g = v_t \pm C_s + \frac{1}{\pi}\sqrt{gL}\left[\frac{(3\epsilon_s/\epsilon + 2)\epsilon_s}{\epsilon_{so}}\right]^{1/2}. \tag{35}$$

For zero gravity and zero terminal velocity, Eq. 35 reduces itself to analogous choking condition for gas flow in the pipe

$$v_g = \pm\text{Sonic velocity}. \tag{36}$$

Equation 35 shows that for large terminal velocities, the choking velocity is higher for the same volume fraction and pseudosonic velocity than it is for smaller particles. The choking velocity in Eq. 35 depends upon the riser height, L. Its contribution is normally of the same order of magnitude as C_s, of the order of 1 m/s. There is no dependence on pipe diameter due to the one-dimensional approximation made in the analysis.

To relate the volume fraction to the prescribed flux, W_s, we used equation (3.10) in Gidaspow's book (1994)

$$\epsilon_s = \frac{W_s/\rho_s}{v_g - v_t}. \tag{37}$$

Further, in Eq. 35 normally $3\epsilon_s/\epsilon < 2$. Substitution of Eq. 37 into Eq. 35 then gives an expression for the maximum carrying capacity of the riser

$$\frac{W_s}{\rho_s} = (v_g - v_t)\left(\frac{\pi^2\epsilon_{so}}{2gL}\right)(v_g - v_t \pm C_s)^2. \tag{38}$$

In Eq. 38 ϵ_{so} was the initial volume fraction in the riser. If it is of the order of 0.2, then the constant $((\pi^2\epsilon_{so})/2)$ is of the order of one.

Equation 38 shows that the flux increases as the cube of the gas velocity at choking, which is qualitatively consistent with the experimental data.

In the preceding analytical solution, the first term of the Ergun equation, Eq. 6, was used to relate the differential change of the pressure drop and bed height. This is valid only for Reynolds numbers less than 10. For higher Reynolds numbers, the second part of the Ergun equation should be used. It is

$$-\frac{dP}{dx} = \frac{1.75\rho}{(\phi d_p)}\frac{\epsilon_s}{\epsilon^3}U_o^2. \tag{39}$$

Then the relative differential change of pressure drop due to a change in the volume fraction is estimated as

$$\frac{d\left(\frac{dP}{dx}\right)}{\frac{dP}{dx}} = [3\epsilon_s/\epsilon + 1]\frac{d\epsilon_s}{\epsilon_s}. \tag{40}$$

The same procedure is used to estimate the frequency of oscillations when the Reynolds number is higher than 10

$$\omega = \left(\frac{g}{x_o}\right)^{1/2}\left[\frac{(3\epsilon_s/\epsilon + 1)\epsilon_s}{\epsilon_{so}}\right]^{1/2}. \tag{41}$$

When the second part of the Ergun equation is used, the choking velocity, Eq. 35, takes the form

$$v_g = v_t \pm C_s + \frac{1}{\pi}\sqrt{gL}\left[\frac{(3\epsilon_s/\epsilon + 1)\epsilon_s}{\epsilon_{so}}\right]^{1/2}. \tag{42}$$

Finally using the same approximations, the maximum carrying capacity of the riser is estimated as

$$\frac{W_s}{\rho_s} = (v_g - v_t)\left(\frac{\pi^2\epsilon_{so}}{gL}\right)(v_g - v_t \pm C_s)^2 \tag{43}$$

This form of the maximum carrying capacity estimate is used for the comparisons made to the experimental data when the Reynolds number is higher than 10.

Granular Temperature of Geldart A, B, and C Particles

In a series of articles, George Cody and collaborators (Cody et al., 1996; Buyevich and Cody, 1998; Cody, 2000) have measured the granular temperature of A, B, and C particles in bubbling fluidized beds, using an acoustic shot-noise tech-

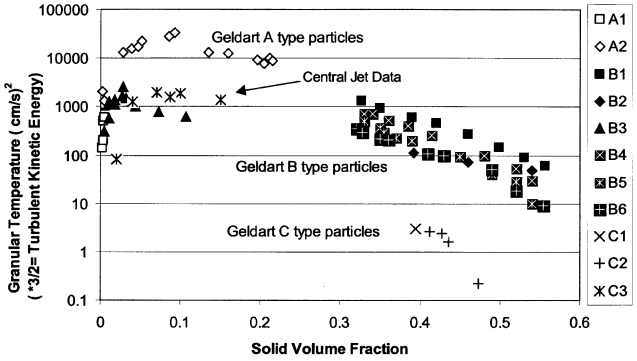

Figure 6. Granular temperature of Geldart type A, B, and C particles.

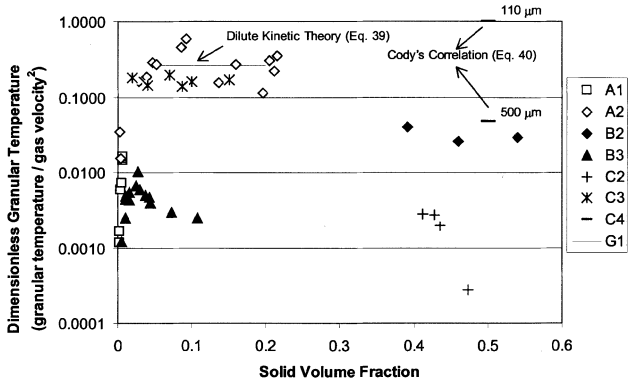

(a)

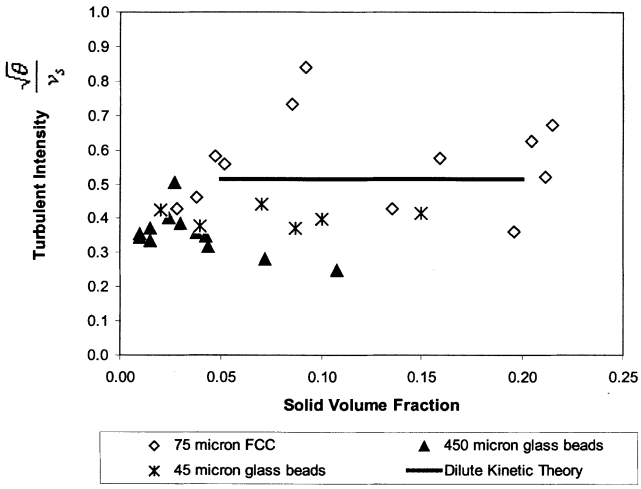

(b)

Figure 7. (a) Dimensionless granular temperature scaled with gas velocity; (b) turbulent intensity in the riser regime scaled with solids velocity.

nique. They used a pizoelectric acceloerometer like the one fully described by Broch (1984). Granular temperature is essentially the random or turbulent kinetic energy of particles. They found that Geldart A particles exhibit an order of magnitude higher granular temperature than the neighboring B glass spheres. Measurements of granular temperature in a riser using a CCD camera like that described by Gidaspow and Huilin (1996, 1998) led to the same conclusions. In the CCD camera technique, the particle velocity is measured by means of the length of a streak divided by the elapsed time. The direction of the velocity is determined by means of a rotating color-coded transparency placed in front of the camera. The granular temperatures for 75-micron FCC and 530-micron glass beads in the IIT riser are given in Figure 6. Also shown are the measurements for 40-micron glass beads done in a rectangular bed with a central jet. Such an arrangement permits the determination of granular temperature under dilute and dense conditions. Details of the apparatus are described in Gidaspow et al. (2001). The figure also depicts the data of other investigators.

The dependence of granular temperature on the particle diameter can be obtained by equating the rate of energy dissipation due to inelastic collisions to the production due to a shear gradient (Gidaspow, 1994). Such an approximation gives

$$\text{Granular temperature} = \frac{1}{15(1-e)}\left(\frac{\partial v_s}{\partial r}\right)^2 d_p^2, \quad (44)$$

where e is the restitution coefficient, v_s is the particle velocity, and d_p is the particle diameter. For a constant gradient of velocity, the equation shows the quadratic dependence of the granular temperature on the particle diameter. Figure 7a shows that this is true for B and C particles in the bubbling regime. An exact comparison would require knowledge of all velocity gradients in the fluidized bed. In the riser, the strange behavior of Geldart A vs. B particles can be explained in terms of the large slip of the B particles. The solid velocity gradient can be approximated as

$$\text{Shear gradient} = (\text{Gas velocity} - \text{Terminal velocity})/\text{Pipe radius}. \quad (45)$$

Thus

$$\text{Granular temperature} = \text{Constant} \times \text{decreasing function of diameter} \times \text{Diameter square}. \quad (46)$$

Hence, due to slip, there exists a maximum with respect to particle diameter. Buyevich and Cody (1998) give a somewhat different hydrodynamic explanation for the maximum granular temperature in a bubbling fluidized bed.

It is possible to obtain a different relationship for the granular temperature. We follow the theory of Sinclair and Jackson (1989). In the developed flow in a riser with flow of elastic particles, the granular temperature balance (Gidaspow, 1994; Jackson, 2000) involves a balance between conduction and generation. In the cylindrical coordinates it is as follows for a constant conductivity, κ, and particle viscosity, μ_s

$$\frac{\kappa}{r}\frac{d}{dr}\left(r\frac{d\theta}{dr}\right) = -\mu_s\left(\frac{\partial v_s}{\partial r}\right)^2. \quad (47)$$

As a limit we had assumed that all dissipation occurs at the wall. We prescribe the wall granular temperature at pipe surface; $r = R$

$$\theta(R) = \theta_w. \tag{48}$$

The solids velocity, v_s, can be approximated as the difference between the gas and the terminal velocity, leading to a lower shear rate for larger particles and a possible explanation for the maximum in Cody and Goldfarb's data (1998). However, here we assume homogeneous flow, as is roughly correct for the flow of FCC particles in the CFB.

We had estimated the FCC viscosity (Miller and Gidaspow, 1992) from the mixture momentum balance

$$\frac{\mu_s}{r}\frac{d}{dr}\left(r\frac{dv_s}{dr}\right) = \frac{dP}{dx} - \rho_m g, \tag{49}$$

and the measurement of the solids radial velocity profile. Then Eq. 49 can be used to obtain the velocity gradient in Eq. 47. Unfortunately the mixture density is a function of the radius r. One can, however, divide the flow into two regions, the core and the dense annulus. Neglecting the thin annular downflow region, integration of Eq. 49 then gives the usual Poiseuille flow. Integration of Eq. 47 then gives a fourth-power dependence of granular temperature on radius, like the thermal temperature rise in Poiseuille flow (Schlichting, 1960). Experimental data obtained in a symmetric IIT riser for fluidization of 530-micron glass beads shows a parabolic particle velocity distribution and a fourth power dependence of granular temperature, as predicted from this theory (Tartan and Gidaspow, 2002). In terms of the mean velocity, $\bar{v}$, the relation between the maximum granular temperature, $\theta_{\max}$, and $\bar{v}_s$ is then the same as the relation between the thermal temperature and the mean velocity

$$\theta_{\max} - \theta_w = \left(\frac{\mu_s}{\kappa}\right)\bar{v}_s^2. \tag{50}$$

Eq. 50 shows that the granular temperature is of the order of the solid velocity squared. In the dilute limit the ratio of viscosity to conductivity is 4/15 (Gidaspow, 1994, table 10.1 and Eq. 9.215). Equation 50 shows the reasonable result that at low velocities, the granular temperature will be correspondingly low. It provides a first-order estimate of the granular temperature and the pseudosonic velocity needed in the present analysis. Note that Cody et al. (1996) empirically find that for the gas superficial velocities greater than twice the minimum fluidization velocity

$$\text{Granular temperature} = \left(\frac{110}{d_p}\right)^2 U_o^2. \tag{51}$$

Cody et al. Eq. 18b

Figure 7a shows a replot of Figure 6, using the gas velocity as a scale factor. For a small slip, the gas and the particle velocities are equal. Observe that for A particles, Eq. 50 approximately predicts the granular temperature. This scale factor does not hold for B particles due to slip and for C particles in the dense region due to cohesion. In the jet region the particle velocity is sufficiently high to overcome cohesion forces. Hence the scaled granular temperature or the turbulence intensity for A and C particles is not sufficiently different.

We estimate the average solids velocity for the B particles by using the slip relation, Eq. 45. Figure 7b shows that the granular temperature scaled with the average solids velocity for A, B, and C particles fall on the same curve, within the experimental error, which is on the order of 50% for B particles. The experimental values are close to the kinetic theory prediction.

Cody's data in the bubbling regime can be explained in a similar manner, approximately. Van Wachem et al. (2001) have plotted solids viscosities and granular conductivities as a function of volume fraction for various theories. These ratios are near one in the bubbling regime. For 110-micron particles, Cody's experimental Eq. 51 and the theoretical Eq. 50 become identical, when one realizes that in Eq. 50 the wall granular temperature is near zero relative to its maximum value and that the average solids velocity is close to experimental superficial velocity. The lower values for the 500-micron particles probably can be explained by slip again. Unfortunately we do not know the solids velocity in Cody's experiments, but know that the slip relation, used in the riser, fails in the bubbling bed due to complex flow patterns.

Both the data of Cody et al. (1996) and the data depicted in Figure 6 have a maximum in granular temperature with respect to solid volume fraction. The decrease in the granular temperature with the solids volume fraction can be explained due to the decrease in the mean free path of the particles. The increase in the granular temperature with the solids volume fraction under dilute conditions is analogous to compression of a gas. Upon compression, the gas gets hot. There exists a sufficient understanding of the granular temperature behavior for us to proceed to make intelligent guesses for unknown systems, as is done in the following section.

Figure 8 shows the estimates for the dimensionless granular temperature for three different sizes. The gas velocity was chosen as the scaling factor, since the solids velocities for the experiments were not known. The granular temperatures of the 75-micron FCC particles were chosen as the basic value, and the dimensionless granular temperatures of the other two sizes were estimated by scaling the values for the FCC parti-

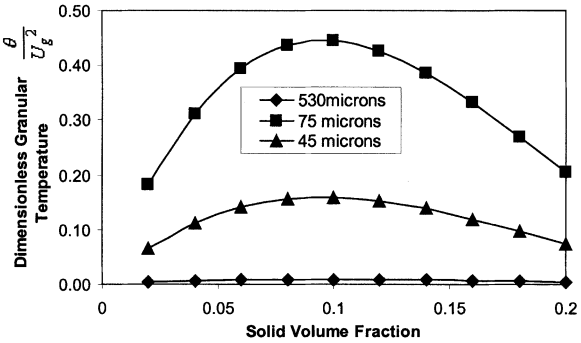

Figure 8. Estimated dimensionless granular temperature from IIT experimental data.

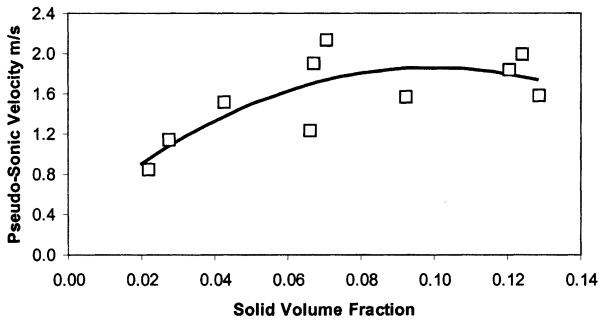

Figure 9. Estimated solids pseudosonic velocity of FCC particles used in the prediction of natural frequency and solids choking velocity.

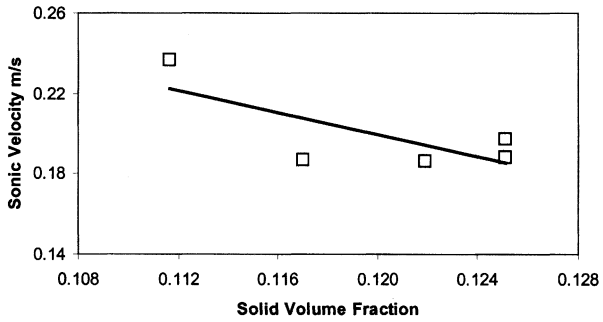

Figure 11. Estimated solids pseudosonic velocity for cork for natural frequency calculations.

cles by the ratio of the particle sizes. It should be noted that the values for the FCC particles are assumed to be maximum based on the values presented in Figure 6. In the next section the same method was used to predict the granular temperature and pseudosonic velocities of the particles in different systems. In the first step, the dimensionless granular temperature of the particles was estimated from the basic graph for FCC particles in Figure 8 and the particle size at each solids volume fraction. Then this value was used to calculate the granular temperature at different superficial gas velocities. Equation 26 was then used to calculate the pseudosonic velocities.

Comparison to Experimental Data

The estimate of the choking velocity and the maximum flux requires the knowledge of the pseudosonic velocity of particles. Based on the equation of state for the FCC particles (Gidaspow and Huilin, 1998), we estimated the pseudosonic velocity shown in Figure 9. The solids volume fraction was estimated from the relation pressure drop, which was equal to the weight of the bed. Using this sonic velocity of particles, Eq. 38 was used to compute the theoretical values of maximum flux divided by density for several superficial gas velocities. In the computation, the bed height was 5.5 m, the terminal velocity was 0.16 m/s, and ϵ_{so} was guessed to be 0.02. The approximate analytical formula, Eq. 38, clearly predicts the trend. The solids lines in Figure 9 and in the later figures represents the best fit through the theoretical points shown.

Recently at NETL, Morgantown, WV, Shaddle et al. (2002) have measured the maximum solids flux for 1,280-micron cork particles in a 15.5-m riser. Again we estimated the solids volume fractions from the measured pressure drops. We guessed the sonic velocity, as shown in Figure 11. With such sonic velocity the agreement between the experiment and theory is quite good (see Figure 12). A comparison of FCC and cork data shows that the flux divided by the density is about a factor of 5 lower for the transport of cork. The actual fluxes were about 2 kg/m^2·s for cork and about 80 kg/m^2·s for FCC for a velocity of about 2.8 m/s. This difference is due to the higher terminal velocity and lower sonic velocity for cork. The low estimated sonic velocity for cork is consistent with our measurements for 500-micron glass beads, which have an order of magnitude lower granular temperature than the FCC particles.

The earliest systematic data for the maximum carrying capacity of various-size particles was obtained in a 3-m riser by Lewis et al. in 1949. Based on our analysis in the previous paragraph of the data in the literature for the granular temperature presented, we estimated the sonic velocity of the three sizes of the particles used by Lewis et al. (1949). The estimates are shown in Figure 13. In this case, the solids volume fractions were given in the article by Lewis et al. (1949). Figure 14 shows a comparison of the maximum carrying capacity divided by the particle density vs. the superficial gas velocity. Equation 38 was used to compute the theoretical values in Figure 14. It is clear that Eqs. 38 and 43 are capable of predicting the choking velocity for short, 3-m, and for tall,

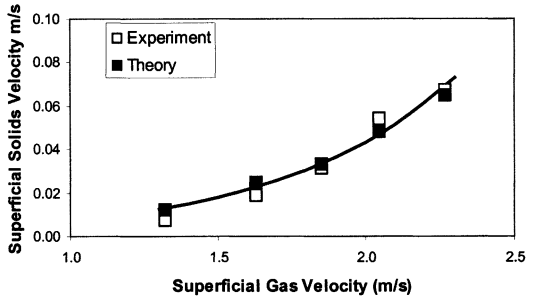

Figure 10. Theoretical prediction of choking velocity for different solids superficial velocities of FCC particles (Takeuchi et al., 1986): [$\epsilon_{so} = 0.02$; $L = 5.5$ m].

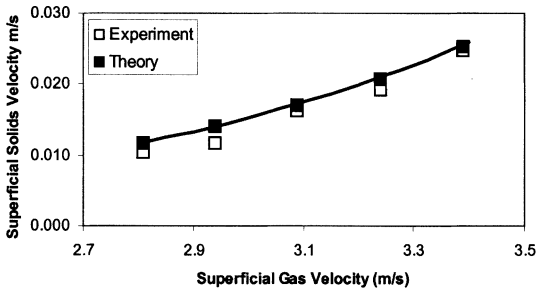

Figure 12. Predictions using present theory vs. experimental data of Shadle et al. (2002): [$\epsilon_{so} = 0.02$; $L = 15.45$ m].

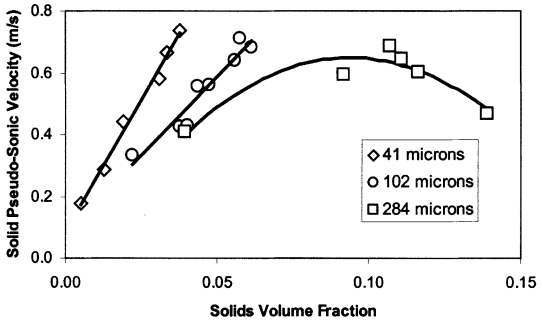

Figure 13. Pseudosonic velocity used for predictions of choking velocity for data of Lewis et al. (1949).

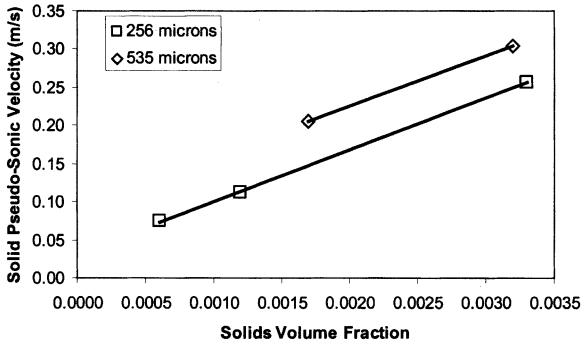

Figure 15. Pseudosonic velocity used for predictions of choking velocity for data of Capes and Nakamura (1973).

15-m, risers. Hence the use of the length of the riser rather than the diameter, sometimes used in literature correlations, is justified.

We applied the theory to the data of Capes and Nakamura (1973) for large dense particles, which have a high terminal velocity. Our estimate of the sonic velocity is shown in Figure 15. At the high superficial gas velocities of Capes and Nakamura, the solids volume fractions are very low. They are at the border of applicability of kinetic theory of granular flow, since at such low concentrations collisions with the wall become important. Figure 16 shows that Eq. 43 can describe the data. Table 4 summarizes all the experimental data used for the comparison to this analytical solution.

Discussion

The approximate theoretical equation for the maximum carrying capacity, Eq. 38, can be used to predict the behavior for Geldart A, B, and C particles. It suggests that for a given gas velocity, the transport will be highest for A particles, since for such particles the sonic velocity is the highest and the terminal velocity is small. For C particles, neglecting the formation of agglomerates due to cohesion, the equation reduces itself to

$$\frac{W_s}{\rho_s} = \left(\frac{\pi^2 \epsilon_{so}}{2gL}\right) v_g^3, \tag{52}$$

since the terminal velocity and the sonic velocity are small for the C particles. Then Eq. 37 shows that

$$\epsilon_s = \left(\frac{\pi^2 \epsilon_{so}}{2gL}\right) v_g^2. \tag{53}$$

Equations 52 and 53 suggest that C particles can be transported at high velocities in a riser. At sufficiently high velocities, the granular temperature may be high enough to overcome cohesive forces that tend to form agglomerates. In practice, C particles are transported at high velocities.

Conclusions

1. It was shown that a multiphase computational fluid-dynamic model is capable of predicting the cyclic operation of a riser near choking conditions consistent with qualitative experimental observations. Previously this model with experimental particulate viscosity as an input had predicted the core–annular structure of flow in agreement with experimental data. The model also predicted the two types of flow regimes in the riser, one having a parabolic flux profile, and the second with an inverted parabola and maximum flux near the wall (Sun and Gidaspow, 1999). The latter flow regime

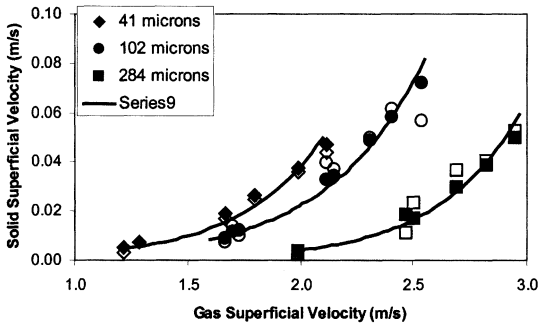

Figure 14. Experimentally measured (open symbols) vs. theory predictions (closed symbols) maximum carrying capacity for the data of Lewis et al. (1949): [$\epsilon_{so} = 0.02$ for different sizes; $L = 3.05$ m].

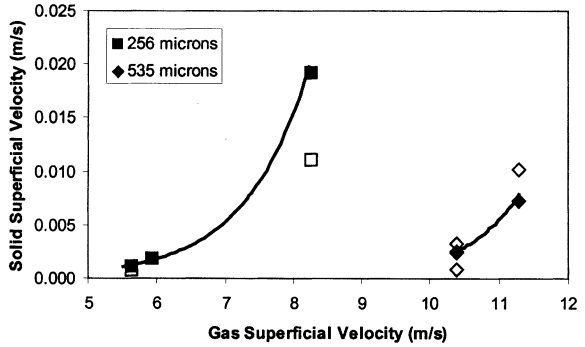

Figure 16. Experimentally measured (open symbols) vs. theory predictions (closed symbols) maximum carrying capacity for the data of Capes and Nakamura (1973): [$\epsilon_{so} = 0.001$, 0.002 for different sizes; $L = 5.5$ m].

Table 4. Summary of the Maximum Carrying-Capacity Data

Figure No.	9	11	13			15	
Reference	Takeuchi et al. (1986)	Shadle et al. (2002)	Lewis et al. (1949)			Capes and Nakamura (1973)	
Bed height (m)	5.5	15.45	3.05			5.5	
Particle size (μm)	57	1,280	41	102	284	256	535
Particle density (kg/m^3)	1,188	189	155	155	152	7,510	7,850
Terminal velocity (m/s)	0.16	0.86	0.16	0.77	1.4	4.0	8.3
Average Bed Inventory, ϵ_{so}(—)	0.02	0.02	0.02	0.02	0.02	0.001	0.002
Reynolds no.	1	163	1	12	60	152	656

occurs at high gas velocities and high solid fluxes, typical of the operation of commercial risers.

2. An approximate analytical equation for the maximum carrying capacity of Geldart A, B, and C particles was developed and compared to data in the literature for short and long risers. The physical basis of this derivation is the concept of resonance. It is based on the observation that near choking the pressure oscillations become unbounded.

3. To estimate the pseudosonic velocity in the equation for the maximum carrying capacity, we present newly measured granular temperatures for Geldart A, B, and C particles and various studies in the literature. These temperatures are interpreted in terms of the approximate expressions derived based on kinetic theory of granular flow. In the riser we find that Geldart A particles have the highest granular temperature. This is consistent with the earlier observation of George Cody in bubbling beds.

4. In the riser flow regime, the measured values of the granular temperature for Geldart A, B, and C particles agree with an approximate theoretical equation derived based on the granular flow theory of Sinclair and Jackson (1989).

5. The turbulent intensity in the riser flow regime (2% to 20% solid volume fraction) is roughly 50%, or more than five times higher than for single phase flow in a pipe. This enhanced turbulence explains the desirable mixing characteristics of circulating fluidized beds.

Acknowledgment

This study was supported by National Science Foundation Grant CTS-0086250 and by the Dow Corning Corporation through the Multiphase Fluid Dynamics Research Consortium.

Notation

C_s = pseudosonic velocity of particles
D = pipe diameter
d_p = particle diameter
e = restitution coefficient
f = frequency of oscillation
F = flux
g = gravitational acceleration
L = bed diameter
P = pressure
R = pipe diameter
r = radial coordinate
Re = Reynolds number, $d_p v_t/\nu_g$
t = time
U_o = inlet superficial gas velocity
v = velocity
W_s = solids mass flow per unit area
x = direction of flow
y = perpendicular direction to flow
z = axial coordinate

Greek letters

β = drag coefficient
ϵ = volume fraction
θ = granular temperature
κ = granular temperature conductivity
μ = viscosity
ν = kinematic viscosity
ρ = density

Subscripts

g = gas
m = mixture
o = average inventory or initial value
p = particle
s = solid
t = terminal velocity
w = wall property

Literature Cited

Avidan, A. A., "Fluid Catalytic Cracking," *Circulating Fluidized Beds*, J. R. Grace, A. A. Avidan, and T. M. Knowlton, eds., Blackie, London, p. 466 (1997).
Avidan, A., "Fluidized Bed Reactor, Scale-up and Scale-down," PSRI Annual Meeting, Chicago (2001).
Baeynes, J., and D. Geldart, "An Investigation into Slugging Fluidized Beds," *Chem. Eng. Sci.*, **29**, 255 (1974).
Benyahia, S., H. Arastoopour, and T. M. Knowlton, "Prediction of Solids and Gas Flow Behavior in a Riser Using a Computational Multiphase Flow Approach," *Proc. Engineering Foundation Conf. on Fluidization*, Durango, CO, p. 493 (1998).
Benyahia, S., and H. Arastoopour, "Prediction of Flow Behavior for Challenge Problem 2," *Fluidization X*, China (2001).
Bi, H. T., J. R. Grace, and J.-X. Zhu, "Types of Choking in Vertical Pneumatic Systems," *Int. J. Multiphase Flow*, **19**, 1077 (1993).
Broch, J. T., *Mechanical Vibration and Shock Measurements*, Brüel and Kjaer, Denmark (1984).
Buyevich, Y. A., and G. D. Cody, "Particle Fluctuations in Homogeneous Fluidized Beds," *Preprints for Brighton World Congr. on Particle Technology*, Vol. 3, Brighton, UK (1998).
Campbell, C. S., and D. G. Wang, "Particle Pressure in Gas Fluidized Beds," *J. Fluid Mech.*, **227**, 495 (1991).
Capes, C. E., and K. Nakamura, "Vertical Pneumatic Conveying: An Experimental Study with Particles in the Intermediate and Turbulent Flow Regime," *Can. J. Chem. Eng.*, **51**, 31 (1973).
Chen, J. C., W. Polashenski, and K. Tuzla, "Normal Solid Stress in Fluidized Beds," *Fluidization Preprints, Annual Meeting*, AIChE, New York, p. 14 (1994).
Cody, G. D., and D. J. Goldfarb, "Bifurcation in Particle Granular Temperature of Monodispersed Glass Spheres at the Geldart A/B Transition," *Fluidization IX*, L. S. Fan and T. M. Knowlton, eds., Engineering Foundation, New York, p. 53 (1998).
Cody, G. D., D. J. Goldfarb, G. V. J. Storch, and A. N. Norris, "Particle Granular Temperature in Gas Fluidized Beds," *Powder Technol.*, **87**, 211 (1996).
Cody, G. D., "Particle Fluctuation Velocity in Gas Fluidized Beds—Fundamental Models Compared to Recent Experimental Data," *Mater. Res. Soc. Symp. Proc.*, **627** (2000).
Gidaspow, D., *Multiphase Flow and Fluidization: Continuum and Kinetic Theory Descriptions*, Academic Press, Boston (1994).
Gidaspow, D., and L. Huilin, "Collisional Viscosity of FCC Particles in a CFB," *AIChE. J.*, **42**, 2503 (1996).

Gidaspow, D., and L. Huilin, "Equation of State and Radial Distribution Function of FCC Particles in a CFB," *AIChE J*, **44**, 279 (1998).
Gidaspow, D., L. Huilin, and R. Mostofi, "Large Scale Oscillations or Gravity Waves in Risers and Bubbling Beds," *Proc. Engineering Foundation Conf. on Fluidization*, M. Kwauk, J. Li, and W.-C. Yang, eds., New York, p. 317 (2001).
Gidaspow, D., and R. Mostofi, "CFD Simulations of Risers: Challenge Problem 2 from a Modeler's Perspective," Multiphase Fluid Dynamics Research Consortium, Salt Lake City, UT (2001).
Gidaspow, D., M. R. Mostofi, and X. Wu, "Turbulence of Particles in a CFB and Slurry Bubble Columns Using Kinetic Theory," *Fluidization Preprints, AIChE Meeting*, AIChE, New York (1999).
Guenther, C., M. Syamlal, and T. O'Brien, "Prediction of Flow Behavior for Challenge Problem 2," *Fluidization X*, China (2001).
Jackson, R., *The Dynamics of Fluidized Particles*, Cambridge Univ. Press, Cambridge (2000).
Jung, J., PhD Thesis, Illinois Institute of Technology, Chicago, IL, in progress (2002).
Knowlton, T. M., and D. M. Bachovchin, "The Determination of Gas-Solids Pressure Drop and Choking Velocity as a Function of Gas Density in a Vertical Pneumatic Conveying Line," *Fluidization Technology,* Vol. II, D. L. Keairns, ed., Hemisphere, Washington, DC, p. 253 (1976).
Kuippers, J. A. M., B. P. B. Hoomans, and W. P. M. van Swaaij, "Hydrodynamic Models for Gas-Fluidized Beds and Their Role for Design and Operation of Fluidized Bed Reactors," *Fluidization IX,* L. S. Fan and T. M. Knowlton, eds., Engineering Foundation, New York, p. 15 (1998).
Leung, L. S., "The Ups and Downs of Gas-Solid Flow—A Review," *Fluidization*, J. R. Grace and J. M. Matsen, eds., Plenum Press, New York, p. 25 (1980).
Lewis, W. K., E. R. Gilliland, and W. C. Bauer, "Characteristics of Fluidized Particles," *Ind. Eng. Chem.,* **41**, 1104 (1949).
Mathiesen, V., T. Solberg, H. Arastoopour, and B. H. Hjertager, "Experimental and Computational Study of Multiphase Gas/Particle Flow in a CFB Riser," *AIChE J.*, **45**, 2503 (1999).
Miller, A., and D. Gidaspow, "Dense, Vertical Gas-Solid Flow in a Pipe," *AIChE J.*, **11**, 1801 (1992).
Morse, P. M., and H. Feshbach, *Methods of Theoretical Physics*, McGraw-Hill, New York (1953).
Polashenski, W. J., and J. C. Chen, "Measurement of Particle Phase Stresses in Fast Fluidization," *Ind. Eng. Chem. Res.*, **38**, 705 (1999).
Satija, S., J. B. Young, and L.-S. Fan, "Pressure Fluctuations and Choking Criterion for Vertical Pneumatic Conveying of Fine Particles," *Powder Technol.*, **43**, 257 (1985).
Savage, S. B., "Streaming Motions in a Bed of Vibrationally Fluidized Dry Granular Material," *J. Fluid Mech.,* **194**, 457 (1988).
Schlichting, H., *Boundary Layer Theory*, McGraw-Hill, New York, (1960).
Shadle, L. J., E. R. Monazam, and J. S. Mei, "Circulating Fluid Bed Operating Regimes," Int. Conf. on Circulating Fluidized Beds, Niagara Falls, Canada (2002).
Sharma, B., Masters Project, Illinois Institute of Technology, Chicago, IL, unpublished (2002).
Sinclair, J. L., and R. Jackson, "Gas-Solid Flows in a Vertical Pipe with Particle-Particle Interaction," *AIChE J.*, **35**, 1473 (1989).
Squires, A. M., M. Kwauk, and A. A. Avidan, "Fluid Beds: At Last, Challenging Two Entrenched Practices," *Science*, **230**, 1329 (1985).
Sun, B., and D. Gidaspow, "Computation of Circulating Fluidized Bed Riser Flow for the Fluidization VIII Benchmark Test," *Ind. Eng. Chem. Res.*, **38**, 787 (1999).
Takeuchi, H., T. Hirama, T. Chiba, J. Biswas, and L. S. Leung, "A Quantitative Definition and Flow Regime Diagram for Fast Fluidization," *Powder Technol.*, **47**, 195 (1986).
Tartan, M., and D. Gidaspow, "Measurement of Radial Granular Temperature Distribution in a Riser and a Comparison to an Analytical Solution," Multiphase Fluid Dynamics Research Consortium, Purdue Univ., West Lafayette, IN (2002).
Thompson, A. S., "Instabilities in a Coal Burning Fluidized Bed," Oak Ridge National Laboratory Rep., Oak Ridge, TN (1978).
Thompson, T., Semi-Annual Meeting and Review, Albuquerque, NM (2000), (tbthompson@dow.com).
Tolstoy, I., *Wave Propagation*, McGraw-Hill, New York (1973).
Van Wachem, B. G. M., J. C. Schouten, C. M. van den Bleek, R. Krishna, and J. L. Sinclair, "Comparative Analysis of CFD Models of Dense Gas-Solid Systems," *AIChE J.*, **47**, 1035 (2001).
Verloop, J., and P. M. Heertjes, "Periodic Pressure Fluctuations in Fluidized Beds," *Chem. Eng. Sci.,* **29**, 1035 (1974).
Yang, W.-C., "A Mathematical Model of Choking Phenomenon and a Mathematical Model for Predicting Choking Velocity and Choking Voidage," *AIChE J.,* **21**, 1013 (1975).
Yang, W.-C., "Criteria for Choking in Vertical Conveying Lines," *Powder Technol.,* **35**, 143 (1983).
Yousfi, Y., and G. Gau, "Aerodynamique de l'Écoulement Vertical de Suspensions Cencentrées Gaz-Solidex: I. Régimes d'Écoulement et Stabilité Aerodynamique," *Chem. Eng. Sci.,* **29**, 1939 (1974).
Zenz, F. A., and D. F. Othmer, *Fluidization and Fluid-Particle Systems*, Reinhold, NewYork (1960).

Manuscript received Oct. 23, 2001, and revision received Sept. 24, 2002.